



LAWRENCE
LIVERMORE
NATIONAL
LABORATORY

Calibration of the OHREX high-resolution imaging crystal spectrometer at the Livermore EBIT

N. Hell, P. Beiersdorfer, E. W. Magee, G. V. Brown

June 7, 2016

High Temperature Plasma Diagnostics Conference
Madison, WI, United States
June 5, 2016 through June 9, 2016

Disclaimer

This document was prepared as an account of work sponsored by an agency of the United States government. Neither the United States government nor Lawrence Livermore National Security, LLC, nor any of their employees makes any warranty, expressed or implied, or assumes any legal liability or responsibility for the accuracy, completeness, or usefulness of any information, apparatus, product, or process disclosed, or represents that its use would not infringe privately owned rights. Reference herein to any specific commercial product, process, or service by trade name, trademark, manufacturer, or otherwise does not necessarily constitute or imply its endorsement, recommendation, or favoring by the United States government or Lawrence Livermore National Security, LLC. The views and opinions of authors expressed herein do not necessarily state or reflect those of the United States government or Lawrence Livermore National Security, LLC, and shall not be used for advertising or product endorsement purposes.

Calibration of the OHREX high-resolution imaging crystal spectrometer at the Livermore Electron Beam Ion Traps^{a)}

N. Hell,^{1,2} P. Beiersdorfer,¹ E. W. Magee,¹ and G. V. Brown¹

¹⁾Lawrence Livermore National Laboratory, Livermore, CA 94550, USA

²⁾Dr. Remeis-Sternwarte & ECAP, Universität Erlangen-Nürnberg, 96049 Bamberg, Germany

(Dated: presented 6 June 2016, accepted 2 July 2016)

We report the calibration of the Orion High-Resolution X-ray (OHREX) imaging crystal spectrometer at the EBIT-I electron beam ion trap at Livermore. Two such instruments, dubbed OHREX-1 and OHREX-2, are fielded for plasma diagnostics at the Orion laser facility in the United Kingdom. The OHREX spectrometer can simultaneously house two spherically bent crystals with a radius of curvature of $r=67.2$ cm. The focusing properties of the spectrometer allow both for larger distance to the source due to the increase in collected light and for observation of extended sources. OHREX is designed to cover a 2.5–3 degree spectral range at Bragg angles around 51.3 degree. The typically high resolving powers at these large Bragg angles are ideally suited for line shape diagnostics. For instance, the nominal resolving power of the instrument (> 10000) is much higher than the effective resolving power associated with the Doppler broadening due to the temperature of the trapped ions in EBIT-I. The effective resolving power is only around 3000 at typical EBIT-I conditions, which nevertheless is sufficient to set up and test the instrument's spectral characteristics. We have calibrated the spectral range for a number of crystals using well known reference lines in first and second order, and derived the ion temperatures from these lines. We have also made use of the $50 \mu\text{m}$ size of the EBIT-I source width to characterize the spatial focusing of the spectrometer.

I. INTRODUCTION

Already since the early times of laser-produced plasma studies have the conditions in these plasmas been diagnosed by means of X-ray spectroscopy¹. Typically, in these plasmas the high electron density causes Stark broadening and its value is derived from the line profiles of suitable X-ray lines, while the electron temperature is inferred from the relative intensity of resonance lines to their dielectronic recombination satellites^{2–5}. To measure the line shape and resolve the forest of satellite lines, X-ray spectrometers with high resolution and a large enough energy coverage are necessary. The Orion laser facility⁶ in the United Kingdom, where systematic studies of high energy density plasmas are conducted, adds the need for large effective area, as its high-powered short-pulse laser produces very small plasmas of order $30\text{--}100 \mu\text{m}$ that radiate only for a few picoseconds, thus reducing the number of emitted photons compared to large, long-pulse laser facilities. Therefore, a new imaging crystal spectrometer has been fielded at Orion, dubbed the Orion High-Resolution X-ray (OHREX) spectrometer⁷.

To maximize the signal-to-noise ratio of the diffracted X-rays on the detector, OHREX adopts design parameters from spherically bent crystal spectrometers used at tokamaks^{8–11}, where the spatial focus is required to coincide on the detector plane with the spectral focus of the Johann geometry, i.e., $q = R_c \sin \theta$ with crystal radius of curvature R_c and Bragg angle θ . The source position

then follows from the focal relations of a spherical mirror and can only be in focus for $\theta > 45^\circ$.

Another key feature of the OHREX is the simplicity of its setup: the instrument is designed around a fixed nominal Bragg angle of 51.3° and corresponding fixed source distance to eliminate the need for time-consuming *in situ* alignment and focusing when the instrument is set up for a new spectral range. Different spectral regions are accessible by choice of crystal based on lattice spacing rather than through changes to the instrument setup. To allow for easy access when switching crystals and to accommodate the large Bragg angle, the OHREX main body is located outside the Orion target chamber, requiring a radius of curvature of $R_c = 67.2$ cm for the crystals. The two crystals that can be housed simultaneously are installed and removed together with their respective mounting plates. Crystal alignment and characterization of their covered spectral range can therefore be done offline at another X-ray source. In this contribution, we describe the calibration of several quartz crystals used in OHREX at the Livermore electron beam ion traps EBIT-I and SuperEBIT^{12,13}.

II. EXPERIMENTAL SETUP FOR CALIBRATION

In an EBIT, X-rays are emitted following the interaction of beam electrons with trapped ions. The ions are confined in a 2 cm long cylindrical trap defined axially through a set of three electrodes and radially by the space charge potential of the electron beam, which for the Livermore traps is compressed to a diameter of $50 \mu\text{m}$ by a 3 T magnetic field. Since EBIT is a relatively weak X-ray source and extended exposures are necessary to measure the spectra with a crystal spectrometer, the image plate ($75 \mu\text{m}$ spatial resolution) that serves as OHREX's de-

^{a)}Contributed paper published as part of the Proceedings of the 21st Topical Conference on High-Temperature Plasma Diagnostics, Madison, Wisconsin, June, 2016.

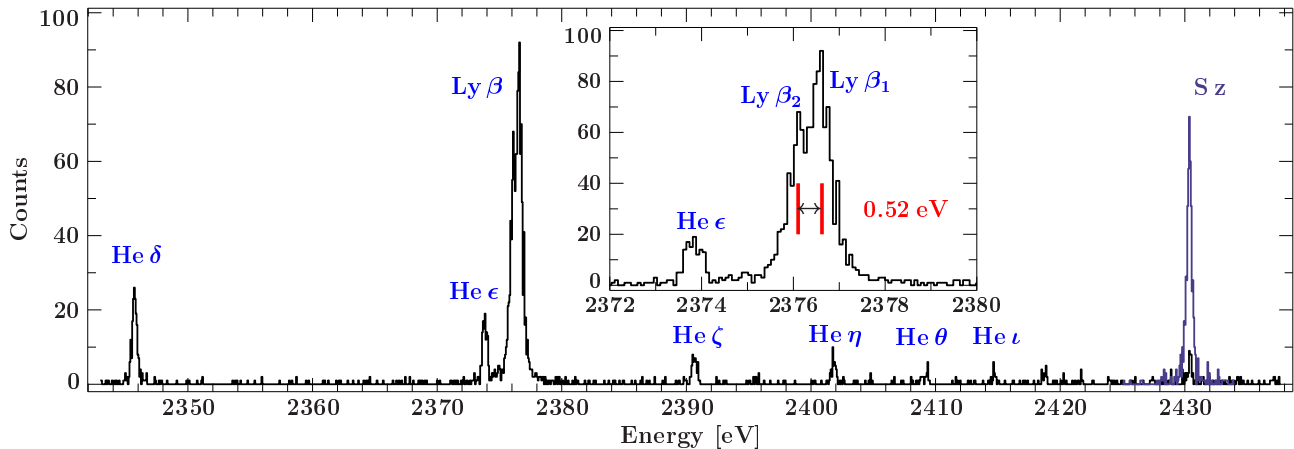


FIG. 1. Calibration spectrum of He- and H-like Si recorded with OHREX using a quartz $10\bar{1}1$ crystal at SuperEBIT. The He-like S line z is shown as well.

tector at Orion is substituted by a charge-coupled device (CCD) detector with an 1300×1340 array of $20 \times 20 \mu\text{m}^2$ pixels at EBIT.

For point sources such as the Orion laser-produced plasma, OHREX is insensitive to the exact focal length both in the spatial and spectral directions. The cylindrical trap, however, makes EBIT a line source. To ensure highest achievable spectral resolution at EBIT, OHREX therefore is at first mounted with the plane of dispersion perpendicular to the electron beam such that the small beam width is focused in the spectral direction, while the trap length is demagnified into an image about 200 pixels wide (cross-dispersion) on the CCD chip.

Due to the small count rates of the experiment, multiple exposures may be necessary to collect sufficient data for calibration. The spectra are extracted from several time-integrated CCD images by a special filtering technique that detects individual photon events. The filter assumes that it is unlikely for two photons to hit the detector in the same or neighboring pixels during a single exposure and only counts pixels that have the maximum pulse height value of the 3×3 pixel array around it. Additionally, the pulse heights are filtered for a narrow range around the pulse heights corresponding to the energies of the observed photons to discriminate against cosmic rays. The extracted spectra, therefore, have very low background.

The high spatial resolution of the CCD detector allows us to assess the spatial focusing of the spectrometer using the width of the electron beam. To do this, we rotated the OHREX such that the plane of dispersion is parallel to the electron beam. In this orientation, with the spectrometer's spatial demagnification factor of $5:1^7$, it should theoretically be possible to focus the image of the beam width down to a single pixel in the spatial direction. However, the best focus we could achieve adjusting the distance to the detector, while the source distance remains fixed, resulted in an image spanning about 9 pixels or about $180 \mu\text{m}$. This width is slightly larger than the highest resolution of the image plates employed at Orion, which means that there is no loss in resolving power from

the detector.

For very weak calibration spectra the smaller spatial focus helps to identify the position of the image on the chip. Additionally, in cases such as, e.g., H-like Mn Ly α observed in second order on a quartz $11\bar{2}0$ crystal, where the photon energy and cosmic rays yield a similar detector response, the smaller image region to be extracted with the parallel setup can greatly reduce the background from cosmic rays. But note that here, due to the long trap, i.e., source size, already small deviations of the detector position from the spectral focal length can deteriorate the spectral resolution of the spectrometer.

III. CALIBRATION RESULTS

Using the OHREX setup at SuperEBIT and EBIT-I, we tested a number of different quartz crystals for the correct alignment at a nominal 51.3° Bragg angle in their mounting plates and for the spectral range covered. Table I lists the examined quartz cuts, the measured reference lines used for calibration, the diffraction order of the observed lines, and the orientation of OHREX relative to the beam. The quartz $10\bar{1}1$ crystal covers the energy range around H-like Si Ly β , which is surrounded by the Rydberg series of He-like Si and close to the He-like S line z. Since of all the tested crystals it shows the largest number of possible calibration lines, which are spread evenly across the entire observed spectral range, we collected the most statistics for the calibration of this crystal and use it to determine the shape of the dispersion. Figure 1 shows the recorded Si calibration spectrum with clear line features of He-like Si transitions up to $n = 8 \rightarrow 1$ (He- η) and indications of even higher order members of the series. As the inset shows, Si Ly β_1 and Ly β_2 are just about resolved, determining the spectral resolution to slightly better than 0.52 eV^{14} . This corresponds to a resolving power of about 4600, much lower than the intrinsic resolution of the quartz crystal.

The line shape is best described by a Voigt profile. The spectral range is determined by fitting a polynomial to

the Bragg angles θ of the reference lines as a function of their line centers in detector channels. The angles are derived through Bragg's law $n\lambda = 2d_n \sin \theta$, where $d_n = d(1 - (2d)^2/n^2 \cdot \delta/\lambda^2)$ is the diffraction order n dependent version of the lattice spacing d corrected for index of refraction effects and $\delta/\lambda^2(\text{SiO}_2) = 3.57 \cdot 10^{-6} \text{ \AA}^{-2}$ is the wavelength independent correction term for quartz¹⁵. While we only use the strong lines S z and Si He δ , He ϵ , Ly β_1 and Ly β_2 for calibration, the resulting line centers of the weak features Si He ζ and He η can be used to test its accuracy. We find that the dispersion is best described by a polynomial of 2nd order. A 3rd order polynomial fitted to the five strong lines adds too much curvature between Si Ly β and S z, but closely traces the shape of the 2nd order polynomial if fitted to all seven lines. The 2nd order polynomial, therefore, leads to a more reliable energy scale when the reference lines are unevenly spaced across the spectral range and, consequently, is used to model the dispersion of all examined crystals.

EBIT operates at densities in the coronal limit, i.e., at much lower densities than the Orion laser, where Stark broadening is not an issue. In fact, the only relevant line broadening mechanism is Doppler broadening due to the temperature of the trapped ions. Since the intrinsic resolving power $\lambda/\Delta\lambda$ of quartz crystals typically exceeds 10 000²¹ and the chosen crystals have very uniform focussing quality^{22,23}, OHREX has very high nominal resolving power and the spectral line widths measured at EBIT are dominated by the Doppler broadening. Table I therefore also lists the full width at half maximum (FWHM) of just the Gaussian component ΔE_G of the fitted Voigt profiles as well as the FWHM ΔE_V of the whole Voigt, and the respective translation into ion temperature for each of the calibration lines. The Gaussian widths constitute only a lower limit for the ion temperature, since both the natural line width and the spectrometer response have only very minor contributions to these lines.

Overall, the measured temperatures are typical for EBIT²⁴⁻²⁷ and the temperatures derived from different lines of the same ion within one measurement are consistent with each other within the uncertainties. However, there are two caveats. Firstly, in case of the quartz 10 $\bar{1}0$ cut, the Si K edge of the crystal at 1839 eV falls right into the energy range covered by OHREX in first order, strongly changing the crystal reflectivity in that region. While the Li-like line q at 1845 eV thus appears to be suppressed, the Si line z at 1839.45 eV is still visible in the spectrum, albeit with an impact to its line shape: if fitted with a Gaussian line profile, the FWHM of Si z is half as large as for Si w. With the Voigt profile, the Gaussian widths are comparable between the two lines and the differences of the crystal response are picked up by the Lorentzian profile instead, where the Lorentzian width of Si w is significantly larger than for Si z. We therefore do not recommend to use the quartz 10 $\bar{1}0$ crystal in first order for plasma diagnostics with OHREX unless the lines of interest are below and far from the edge.

TABLE I. List of calibration lines (transition energy E_{ref} , observed in diffraction order n) for various quartz crystals mounted with the plane of dispersion perpendicular (\perp) or parallel (\parallel) to the electron beam. The calibrated spectra are fit with Voigt profiles and the ion temperature T_{ion} in EBIT is derived from the FWHM of just the Gaussian component ΔE_G and the full Voigt profile ΔE_V , respectively. All energies and temperatures are in units of eV.

Line	n	E_{ref}	ΔE_G	T_{ion}	ΔE_V	T_{ion}
Quartz 10$\bar{1}1$ (\perp)						
Si He δ	1	2345.709 ^a	0.35(12)	107(73)	0.44(09)	167(65)
Si He ϵ	1	2373.786 ^a	0.35(07)	101(41)	0.41(07)	138(48)
Si Ly β_1	1	2376.104 ^b	0.28(09)	67(44)	0.51(06)	220(47)
Si Ly β_2	1	2376.624 ^b	0.28(09)	67(44)	0.51(06)	220(47)
S z	1	2430.347 ^c	0.28(09)	64(42)	0.45(07)	159(46)
Quartz 10$\bar{1}0$ (\perp)						
Si w	1	1865.000 ^c	0.38(28)	196($^{+342}_{-182}$)	0.66(18)	587(328)
Si z	1	1839.448 ^c	0.45(12)	278(146)	0.47(10)	303(127)
Ar He β	2	3683.854 ^d	1.06(24)	553(251)	1.07(25)	567(265)
Quartz 11$\bar{2}0$ (\perp)						
Cl He β	1	3271.543 ^d	0.92(12)	467(120)	1.02(08)	574(93)
Mn Ly α_2	2	6423.561 ^e	1.25(28)	347(157)	1.57(23)	551(156)
Mn Ly α_1	2	6441.665 ^e	0.87(28)	168(110)	1.20(22)	321(114)
Quartz 11$\bar{2}0$ (\parallel)						
Cl He β	1	3271.543 ^d	0.92(19)	475(194)	1.09(15)	661(182)
Mn Ly α_2	2	6423.562 ^e	1.53(43)	524(290)	1.67(26)	624(193)
Mn Ly α_1	2	6441.665 ^e	2.12(26)	999(245)	2.12(23)	999(227)
Quartz 21$\bar{3}1$ (\parallel)						
V w	1	5205.330 ^f	1.29(28)	526(229)	1.32(18)	550(148)
V x	1	5188.861 ^f	–	–	–	–
V y	1	5180.297 ^f	–	–	–	–
V z	1	5153.897 ^f	1.03(22)	342(146)	1.05(15)	355(103)
V q	1	5172.474 ^f	1.1(4)	387(282)	1.12(21)	402(151)

Notes: ^aVerner, Verner, and Ferland¹⁶; ^bGarcia and Mack¹⁴; ^cDrake¹⁷; ^dJohnson and Soff¹⁸; ^eVainshtein and Safronova¹⁹ corrected for ground state of Drake¹⁷; ^fBeiersdorfer *et al.*²⁰.

Secondly, the quartz 11 $\bar{2}0$ crystal was used both with the dispersion plane of OHREX set up perpendicular to the electron beam and in the parallel configuration during a separate measurement. As seen from Table I, the measured widths of the Mn lines in the parallel setup are larger than in the perpendicular setup despite similar EBIT conditions during the two measurements. This indicates that the Mn lines were not optimally focused in the spectral direction during this measurement in the parallel setup, which, because of the macroscopic trap length, is much more sensitive to the focal quality than the perpendicular setup, such that the line width was not solely due to the ion temperature. The likely reason is that the focusing was done on the stronger Cl He β line, whose Bragg angle is about 1° different from the Mn lines, and the focal length $q = R_c \sin \theta$ changes by a few mm over this spectral range. Since the laser-produced plasmas at Orion are point sources, not line sources, the orientation of OHREX is irrelevant and focusing issues do not affect its plasma diagnostic capabilities at Orion.

TABLE II. Observable energy range of the OHREX spectrometer, mounted with a CCD at EBIT or with a larger image plate at Orion, for various crystals (lattice spacing²⁸ $2d$) in 1st and 2nd diffraction order around the photon energy at a nominal Bragg angle of 51.3° .

Crystal	$2d$ [Å]	diff. order	$E(51.3^\circ)$		Range [eV]	
			[eV]	EBIT	Orion ⁷	
Quartz 10 $\bar{1}$ 1	6.687	1	2376	95	150	
		2	4752	189	300	
Quartz 10 $\bar{1}$ 0	8.512	1	1867	75	110	
		2	3733	130	260	
Quartz 11 $\bar{2}$ 0	4.912	1	3234	127	190	
		2	6469	255	380	
Quartz 21 $\bar{3}$ 1	3.082	1	5155	208	320	
		2	10309	417	640	

Note that the somewhat large uncertainties on the measured line widths are not attributed to the spectrometer setup, but solely due to counting statistic. The primary objectives for the calibration at EBIT were to check the crystal alignment and to gauge the spectral ranges for the crystals to be used at Orion. Both tasks can be accomplished with fairly weak spectra. Therefore, the total exposure times at EBIT were kept relatively short for most spectra. Yet, in most cases the line centroids could be determined to within about one pixel.

IV. CONCLUSION

Table 2 summarizes the spectral energy ranges covered by the spectrometer for use at EBIT and Orion. The constant factor between these two setups is attributed to the larger area of the image plate, while the 1-inch CCD camera does not cover the full range of the crystal. We emphasize that the Quartz 10 $\bar{1}$ 0 crystal has the Si K edge in this energy range, impacting line profile measurements due to the sudden changes in reflectivity close to the edge. This crystal should, therefore, not be used in first order at the Bragg angles employed here.

ACKNOWLEDGMENTS

This work was performed under the auspices of the U.S. DOE by LLNL under Contract DE-AC52-07NA27344 and supported by NASA's APRA Program. N. H. received support from European Space Agency under contract No. 4000114313/15/NL/CB.

¹D. J. Nagel, P. G. Burkhalter, C. M. Dozier, J. F. Holzrichter, B. M. Klein, J. M. McMahon, J. A. Stamper, and R. R. Whitlock, *Phys. Rev. Lett.* **33**, 743 (1974).

²B. A. Hammel, C. J. Keane, D. R. Kania, J. D. Kilkenny, R. W. Lee, R. Pasha, R. E. Turner, and N. D. Delamater, *Rev. Sci. Instrum.* **63**, 5017 (1992).

³B. A. Hammel, C. J. Keane, M. D. Cable, D. R. Kania, J. D. Kilkenny, R. W. Lee, and R. Pasha, *Phys. Rev. Lett.* **70**, 1263 (1993).

⁴C. J. Keane, B. A. Hammel, A. L. Osterheld, and D. R. Kania, *Phys. Rev. Lett.* **72**, 3029 (1994).

⁵R. C. Mancini, C. A. Iglesias, S. Ferri, A. Calisti, and R. Florido, *High Energy Density Physics* **9**, 731 (2013).

⁶N. Hopps, K. Oades, J. Andrew, C. Brown, G. Cooper, C. Danson, S. Daykin, S. Duffield, R. Edwards, D. Egan, S. Elsmere, S. Gales, M. Girling, E. Gumbrell, E. Harvey, D. Hillier, D. Hoarty, C. Horsfield, S. James, A. Leatherland, S. Masoero, A. Meadowcroft, M. Norman, S. Parker, S. Rothman, M. Rubery, P. Treadwell, D. Winter, and T. Bett, *Plasma Phys. Controlled Fusion* **57**, 064002 (2015).

⁷P. Beiersdorfer, E. W. Magee, G. V. Brown, H. Chen, J. Emig, N. Hell, M. Bitter, K. W. Hill, P. Allan, C. R. D. Brown, M. P. Hill, D. J. Hoarty, L. M. R. Hobbs, and S. F. James, *Rev. Sci. Instrum.* **87**, 063501 (2016).

⁸M. Bitter, K. W. Hill, A. L. Roquemore, P. Beiersdorfer, S. M. Kahn, S. R. Elliott, and B. Fraenkel, *Rev. Sci. Instrum.* **70**, 292 (1999).

⁹M. Bitter, K. W. Hill, B. Stratton, A. L. Roquemore, D. Mastrovito, S. G. Lee, J. G. Bak, M. K. Moon, U. W. Nam, G. Smith, J. E. Rice, P. Beiersdorfer, and B. S. Fraenkel, *Rev. Sci. Instrum.* **75**, 3660 (2004).

¹⁰K. W. Hill, M. L. Bitter, S. D. Scott, A. Ince-Cushman, M. Reinke, J. E. Rice, P. Beiersdorfer, M.-F. Gu, S. G. Lee, C. Broennimann, and E. F. Eikenberry, *Rev. Sci. Instrum.* **79**, 10E320 (2008).

¹¹P. Beiersdorfer, J. Clementson, J. Dunn, M. Gu, K. Morris, Y. Podpaly, E. Wang, M. Bitter, R. Feder, K. Hill, D. Johnson, and R. Barnsley, *J. Phys. B* **43**, 144008 (2010).

¹²R. E. Marrs, M. A. Levine, D. A. Knapp, and J. R. Henderson, *Phys. Rev. Lett.* **60**, 1715 (1988).

¹³P. Beiersdorfer, E. Behar, K. R. Boyce, G. V. Brown, H. Chen, K. C. Gendreau, A. Graf, M.-F. Gu, C. L. Harris, S. M. Kahn, R. L. Kelley, J. K. Lepson, M. J. May, P. A. Neill, E. H. Pinnington, F. S. Porter, A. J. Smith, C. K. Stahle, A. E. Szymkowiak, A. Tillotson, D. B. Thorn, E. Träbert, and B. J. Wargelin, *Nucl. Instrum. Methods Phys. Res., Sect. B* **205**, 173 (2003).

¹⁴J. D. Garcia and J. E. Mack, *Journal of the Optical Society of America* **55**, 654 (1965).

¹⁵A. H. Compton and S. K. Allison, *X-rays in Theory and Experiment*, 2nd ed. (D. van Nostrand Company, Inc., 1935).

¹⁶D. A. Verner, E. M. Verner, and G. J. Ferland, *Atomic Data and Nuclear Data Tables* **64**, 1 (1996).

¹⁷G. W. Drake, *Can. J. Phys.* **66**, 586 (1988).

¹⁸W. R. Johnson and G. Soff, *Atomic Data Nucl. Data Tables* **33**, 405 (1985).

¹⁹L. A. Vainshtein and U. I. Safronova, *Phys. Scr.* **31**, 519 (1985).

²⁰P. Beiersdorfer, M. H. Chen, R. E. Marrs, M. B. Schneider, and R. S. Walling, *Phys. Rev. A* **44**, 396 (1991).

²¹A. Burek, *Space Sci. Instrum.* **2**, 53 (1976).

²²K. W. Hill, M. Bitter, L. Delgado-Aparacio, P. Efthimion, N. A. Pablant, J. Lu, P. Beiersdorfer, H. Chen, and E. Magee, *Rev. Sci. Instrum.* **85**, 11D612 (2014).

²³N. R. Pereira, A. T. Macrander, K. W. Hill, E. O. Baronova, K. M. George, and J. Kotick, *Rev. Sci. Instrum.* **86**, 103704 (2015).

²⁴P. Beiersdorfer, V. Decaux, S. R. Elliott, K. Widmann, and K. Wong, *Rev. Sci. Instrum.* **66**, 303 (1995).

²⁵P. Beiersdorfer, V. Decaux, and K. Widmann, *Nucl. Instrum. Methods Phys. Res., Sect. B* **98**, 566 (1995).

²⁶P. Beiersdorfer, A. L. Osterheld, V. Decaux, and K. Widmann, *Phys. Rev. Lett.* **77**, 5353 (1996).

²⁷P. Beiersdorfer, J. R. Crespo López-Urrutia, E. Förster, J. Mahiri, and K. Widmann, *Rev. Sci. Instrum.* **68**, 1077 (1997).

²⁸A. Thompson, D. Attwood, E. Gullikson, M. Howells, K.-J. Kim, J. Kirz, J. Kortright, I. Lindau, Y. Liu, P. Pianetta, A. Robinson, J. Scofield, J. Underwood, G. Williams, and H. Winick, *X-ray Data Booklet*, 3rd ed. (Lawrence Berkeley National Laboratory, University of California, 2009).